OPEN ACCESS
IOP Publishing | London Mathematical Society Nonlinearity

Nonlinearity **34** (2021) 5872–5896 https://doi.org/10.1088/1361-6544/ac0f51

Waves in strongly nonlinear Gardner-like equations on a lattice

Philip Rosenau[1] **and Arkady Pikovsky**[2,3,*]

[1] School of Mathematics, Tel-Aviv University, Tel-Aviv 69978, Israel
[2] Institute of Physics and Astronomy, University of Potsdam, Karl-Liebknecht-Str. 24/25, 14476 Potsdam-Golm, Germany
[3] National Research University, Higher School of Economics, 25/12 Bolshaya Pecherskaya Ulitsa, 603155 Nizhny Novgorod, Russia

E-mail: pikovsky@uni-potsdam.de

Received 24 August 2020, revised 28 May 2021
Accepted for publication 28 June 2021
Published 16 July 2021

Abstract

We introduce and study a family of lattice equations which may be viewed either as a strongly nonlinear discrete extension of the Gardner equation, or a non-convex variant of the Lotka–Volterra chain. Their deceptively simple form supports a very rich family of complex solitary patterns. Some of these patterns are also found in the quasi-continuum rendition, but the more intriguing ones, like interlaced pairs of solitary waves, or waves which may reverse their direction either spontaneously or due a collision, are an intrinsic feature of the discrete realm.

Keywords: nonlinear lattice, solitary wave, Gardner equation, compacton
Mathematics Subject Classification numbers: 37K60, 37K40.

(Some figures may appear in colour only in the online journal)

1. Introduction

As their importance has progressively been realized, strongly nonlinear lattices started to attract in the recent decades an ever growing attention [1–12]. This may be seen as a natural scientific evolution following in the footsteps of what may arguably be considered as a dawn of a nonlinear science: the Fermi–Pasta–Ulam (FPU) problem which, as envisioned by von Neumann, used for the first time the newly born computer to carry a Gedanken experiment, to test

*Author to whom any correspondence should be addressed.
Recommend by Dr Tasso J Kaper.

the long standing hypothesis of energy equipartition of modes in solids due to nonlinearity. Though, given the primordial state of affairs, the studied chain, as solids model, was relatively very simple and short, their results after few years in hibernation led to the birth of the soliton and the chaos theories and, as computational facilities have advanced and spread around the globe, to ever more evolved theories and applications. Chains of coupled elements were introduced and used to simulate more realistic molecular interactions, micro-mechanical arrays, electrical transmission lines, optical lattices or photonic crystals, to name a few. A succinct overview is presented in reference [13], and references therein.

A common feature of the aforementioned systems is the presence of a weakly nonlinear regime wherein the dynamics is determined by both linear and nonlinear parts. For such states one may employ simple nonlinear expressions, though one can hardly expect that the quadratic force assumed by FPU could, apart of very small excitations, reproduce realistic molecular interactions. In fact, the numerical experiments carried a few years later have very clearly revealed that as the employed nonlinearity gained in strength, the recurrence of the initial excitation within the FPU had to be replaced by a far more complex structure. If further arguments were ever needed, those results have clearly pointed to the necessity to probe deeper into the nonlinear regime. In the spring–mass context this amounts to exploration of the truly anharmonic domain which in its ultimate form results in a system without linear waves (the so-called sonic vacuum), with all perturbations of the ground state being genuinely nonlinear. Differently stated, a true understanding of the impact of nonlinearity necessitates a full engagement of the nonlinear regime, rather than as an extension of a weakly nonlinear limit. Using an analogy, to the extent that the infra-red and ultra-violet regimes represent opposite ends of the visible spectrum, the linear/weakly-linear and the genuinely nonlinear regimes may be looked upon as conceptual opposites, each of which should be addressed on its own terms. As a typical signature of a genuinely nonlinear system one may consider the absence of a non-scalable intrinsically small parameter to serve as a reference for a weakly nonlinear dynamics.

Let us recall that aside from the conceptual importance of the genuinely nonlinear limit, many systems by their very nature are *ab initio* essentially nonlinear. The Hertz-like interaction of elastic beads is perhaps the simplest mechanical realization of such a system [1, 2, 14–18]. And whereas in mechanics one typically deals with lattices described by coupled second-order differential equations, strongly nonlinear systems have been also explored within the framework of amplitude equations given via discrete Schrödinger-type equations which are first-order in time [4, 9, 12].

In yet another setup, closer to our present studies, a genuinely nonlinear conservative system emerges in a chain of coupled dissipative oscillators with a limit cycle. In a strongly dissipative regime, where the amplitudes of the oscillators are very stable, one may neglect their variations and derive a closed conservative system for their phases only [3, 6]. Such systems fall under what could be referred to as Kuramoto-type setups and in a clear distinction from the Newton-like chains, are systems that are *first order in time*. In a similar spirit, the Lotka–Volterra chain [11] which originates in prey–predator system is another first-order in time strongly nonlinear lattice.

The problems to be addressed here are a direct offspring of the Kuramoto family of strongly nonlinear first-order in time lattices [3, 6, 19]. Instead of considering lattices of phase variables, with 2π-periodic coupling terms, we focus on lattices with polynomial nonlinearities. For the present purpose we shall restrict our attention to nonlinearities which are the sums of two monomials of opposite signs. In this form they are a discrete analog/extension of the Gardner equation, which is a mixture of the Korteweg–de Vries and the modified Korteweg–de Vries equations [20–22]. The lattice we address may be viewed as a simplified version of a generic phase lattice, allowing us to cope with some of the difficulties we have encountered there, and sure enough similarly to their original antecedents did not fail to produce new and surprising features which we believe are of independent interest.

The plan of the paper is as follows. In section 2 we introduce the basic model. In section 3 we present an analytical treatment of the travelling waves akin to the quasi-continuous, QC, approximation. In sections 4 and 5 we return to the full lattice setup and explore numerically simple and interlaced travelling waves. Simulations of the travelling solitary waves in a lattice are presented in section 6 and reveal a number of fascinating phenomena not seen in the QC. We conclude with a discussion in section 7.

2. The basic model

Consider a genuinely nonlinear conservative lattice with nearest-neighbour interactions:

$$\frac{\mathrm{d}u_k}{\mathrm{d}t} = F(u_{k+1}) - F(u_{k-1}), \quad k = \dots, -1, 0, 1, 2, \dots, \tag{1}$$

where $F(u)$ is a smooth nonlinear function, to be specified in equations (3)–(5) below. To put the addressed problems in perspective, we note that our studies were motivated by chains of conservatively coupled self-sustained (autonomous) oscillators wherein the state variable u is the phase difference between neighbouring oscillators reducing in the simplest case [3, 6, 23] to $F(u) = \cos(u)$. With that particular choice the lattice (1) becomes genuinely nonlinear: linear waves are absent. The evolution of a localized initial wave packet is dominated by solitary waves, the compactons and the kovatons, which are almost compact (they decay at a doubly exponential rate) essentially nonlinear entities. Notably, the model (1) has been recently successfully used to describe complex states in a network of nano-electro-mechanical oscillators [24].

In a previous work [19] using a more general setting for phase waves in a chain of autonomous oscillators, it was assumed that $F(u) = \sin(\alpha - u)$. Though numerical simulations posed no particular difficulty, their direct analysis turned to be challenging, forcing us to turn to their quasi-continuous representation and the resulting partial differential equation (PDE). Yet even there we had to further restrict ourselves to a small amplitude regime which turned to be given by the Gardner equation. This approximation, surprisingly enough, provided a remarkably good qualitative description of the $\alpha \leqslant \pi/2$ domain. Since the periodic nature of $F(u)$ seemed to be the source of the encountered difficulties, we adopt in this paper a simpler setup of a polynomial $F(u)$, which replicates two of the vital singular transitions in the periodic case.

In passing we also note that in a lattice of a finite length N and open boundaries, system (1) is Hamiltonian (the proof, due to Dullin, follows reference [6]). Since for odd N system (1) has an additional integral $K = \sum_{i=1}^{(N+1)/2} u_{2i-1}$, defining the 'potential' $Q(u) = \int F(u')\mathrm{d}u'$, the Hamiltonian of the lattice reads

$$H(q_i, p_i) = \begin{cases} Q(q_1) + \sum_{i=1}^{m} Q(p_i) + \sum_{i=1}^{m-1} Q(q_{i+1} - q_i) + Q(K - s_m) & N = 2m+1, \\ Q(q_1) + \sum_{i=1}^{m} Q(p_i) + \sum_{i=1}^{m-1} Q(q_{i+1} - q_i) & N = 2m. \end{cases} \tag{2}$$

The canonical variables are related to u_i via $p_i = u_{2i}$, $q_i = \sum_{j=1}^{i} u_{2j-1}$. In the original variables the conserved energy can be thus expressed as $E = \sum_i Q(u_i)$.

Returning to our specific problem, we assume a strongly nonlinear Gardner-type lattice as

$$F(u) = mu^n - nu^m, \quad 1 < m < n, \tag{3}$$

with integer m, n (the values of the coefficients are arbitrary and were specified to simplify the analysis). Two typical cases will be analysed:

$$\text{G23:} \frac{\mathrm{d}u_k}{\mathrm{d}t} = 2u_{k+1}^3 - 3u_{k+1}^2 - 2u_{k-1}^3 + 3u_{k-1}^2, \qquad F(u) = 2u^3 - 3u^2, \tag{4}$$

and

$$\text{G35:} \frac{\mathrm{d}u_k}{\mathrm{d}t} = 3u_{k+1}^5 - 5u_{k+1}^3 - 3u_{k-1}^5 + 5u_{k-1}^3, \qquad F(u) = 3u^5 - 5u^3. \tag{5}$$

The G23 model is a direct replica of the original Gardner equation. The G35 model has different symmetries, with its resulting properties being quite different from those of the G23. Note the non-monotone nature of F, with the corresponding potentials Q being non-convex. This will emerge as an essential feature of our model. In the case of strictly convex Q, existence of periodic waves in (1) was established in reference [25].

At this point we note the simple stationary solutions of (1). Since $F(u)$ vanishes at $u^* = \left(\frac{n}{m}\right)^{1/(n-m)}$, any sequence of zeros and u^* forms a stationary solution on the lattice. In particular, one can have stationary 'pulse' solutions $\ldots, 0, u^*, u^*, \ldots, u^*, 0, \ldots$ of an arbitrary length. While the construction of these solutions is trivial, their stability properties are rather complex and depend on both the total length of the lattice and the boundary conditions at its ends. Since we focus on travelling waves, we shall not pursue further these solutions.

In addition to the standard conservation features, the G23 model is invariant under

$$u_k \to 1 - u_k, \tag{6}$$

whereas G35, and any Gmn if both m and n are odd, is invariant under

$$u_k \to -u_k \tag{7}$$

and under

$$u_k \to (-1)^k u_k \quad \text{and} \quad t \to -t. \tag{8}$$

This generates from any given solution an alternating sign solution, referred to as a staggering solution in section 5.1 below. Note that whereas the first two invariant features extend to the quasi-continuum, the third (equation (8)) is obviously an exclusive feature of the discrete realm.

We stress that the novel features of the presented problems are due to the *non-monotonic* nature of the assumed $F(u)$ which is to be contrasted with, say, the widely studied integrable version with $F = \exp(u)$ (the so-called ladder equation equivalent to the Toda lattice), see [26, 27]. More relevant to our problem is the discrete $K(\alpha, \alpha)$ equation with the monomial $F = \gamma u^\alpha$ (cf reference [28]):

$$\frac{\mathrm{d}u_k}{\mathrm{d}t} = \gamma \left(u_{k+1}^\alpha - u_{k-1}^\alpha\right), \quad \text{where } \gamma \text{ is a const.}, \tag{9}$$

which may be viewed as a limiting case of the generic lattice (1) and (3), either for large u, where $\gamma = m$, $\alpha = n$, or for small u, where $\gamma = -n$, $\alpha = m$.

Similarly to the previously studied case $F(u) = \cos(u)$, equations (1) and (3) have a deceptively simple appearance. Their numerical integration is straightforward, but the understanding of the underlying dynamics is a very different matter. Indeed, our ability to analyse nonlinear discrete systems, or better yet, to unfold their coherent structures, is very limited, and far more inferior to our ability to analyse systems represented by PDEs. This naturally leads us to represent the discrete system via the quasi-continuum [28, 29], QC (section 3). Yet this approach has its difficulties, for whereas in weakly nonlinear systems the stationary solution provides a reference level with respect to which one carries the asymptotic expansion, as aforementioned, the present problem, lacks an essential small parameter (the distance between the discrete nodes may be scaled out). Therefore, the adopted QC 'approximation' is not truly asymptotic and its value can be *judged only by its utility*. In the following sections we will demonstrate that, in certain regimes, QC provides an excellent approximation of its discrete antecedent, though elsewhere it turned to be of far more limited use (for discussion of quality of QC in other contexts see our previous works [3–6]).

3. Travelling waves in a quasi-continuum

3.1. The quasi-continuum representation

Replacing the finite differences of the discrete lattice equations with continuous spatial derivatives up to a third order yields the QC representation of the original problem (see references [28] or [29] for a detailed exposition of the desired QC approach and its limitations) of equations (1) and (3):

$$\frac{1}{2}\frac{\partial}{\partial t}u = \frac{\partial}{\partial x}\mathcal{L}^2 F(u) \quad \text{where } \mathcal{L}^2 = 1 + \frac{1}{6}\frac{\partial^2}{\partial x^2}. \tag{10}$$

Similarly to their discrete antecedents, we have the following conservation laws of equation (10):

$$I_1 = \int u\,\mathrm{d}x \quad \text{and} \quad I_3 = \int Q(u)\,\mathrm{d}x \quad \text{where } Q(u) = \int^u F(u')\mathrm{d}u', \tag{11}$$

and an unusual Lagrangian structure

$$L_{\text{agrange}} = \iint \left[\frac{1}{4}\psi_x\psi_t + Q\left(\mathcal{L}\psi_x\right)\right]\mathrm{d}x\,\mathrm{d}t, \tag{12}$$

where $u = \mathcal{L}\psi_x$, which results in the conservation of the momentum $\int \psi_x^2\,\mathrm{d}x$, and in the original variables

$$I_2 = \int u\mathcal{L}^{-2}u\,\mathrm{d}x. \tag{13}$$

3.2. Solitary waves in QC

We now turn our attention to solitary waves $u(s = x - \lambda t)$. Since $F(0) = 0$, then upon one integration we have

$$\frac{1}{2}\lambda u + \left(1 + \frac{1}{6}\frac{\mathrm{d}^2}{\mathrm{d}s^2}\right)F(u) = 0, \tag{14}$$

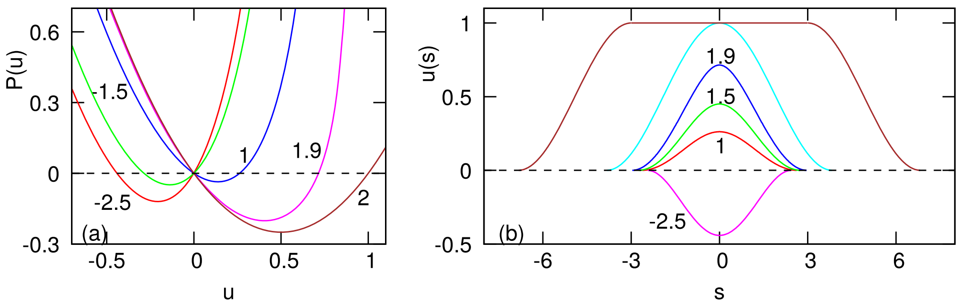

Figure 1. Panel (a): the effective potential $P_{23}(u)/(1-u)^2$ for six values of velocity λ ($\lambda = -2.5$ (red), $\lambda = -1.5$ (green), $\lambda = 1$ (blue), $\lambda = 1.9$ (magenta), $\lambda = 2$ (brown)). Note that only in the last case the effective potential remains bounded. Panel (b): compacton profiles for $\lambda = -2.5$ (magenta), $\lambda = 1$ (red), $\lambda = 1.5$ (green), $\lambda = 1.9$ (blue); the basic kovaton (26) (cyan), and kovaton (27) with $s_0 = 3$ (brown).

or

$$\frac{1}{2}\lambda u + F(u) + \frac{1}{6}\frac{\mathrm{d}}{\mathrm{d}s}F'(u)\frac{\mathrm{d}u}{\mathrm{d}s} = 0. \tag{15}$$

A crucial role is played by the zeros of $F'(u) = mn(u^{n-1} - u^{m-1})$ wherein equation (15) becomes singular at both $u = 0$ and $u = 1$.

Multiplying (15) with $F^{'}(u)u_s$ and integrating once yields the energy integral (since we are after solitary waves the integration constant was discarded)

$$F'^2(u)u_s^2 + 6P(u) = 0 \quad \text{where } P = -\frac{\lambda}{nm}\left(\frac{u^{m+1}}{1+m} - \frac{u^{n+1}}{1+n}\right) + \left(\frac{u^m}{m} - \frac{u^n}{n}\right)^2, \tag{16}$$

and $P(u)$ is the potential. Cancelling u^{2m-2} on both sides leads to

$$\frac{m^2n^4}{6}(1-u^{n-m})^2u_s^2 - \left(\frac{n\lambda}{m(n+1)}\right)\left(\frac{n+1}{m+1} - u^{n-m}\right)u^{3-m} + \left(\frac{n}{m} - u^{n-m}\right)^2 u^2 = 0. \tag{17}$$

The singularity at $u = 0$ which causes degeneracy of the highest order operator and a local loss of uniqueness, allows us to construct compactons—solitary solutions with a compact support. Indeed, since the uniqueness of solutions of (16) is violated at $u = 0$, one may 'glue' there the nontrivial solution of (17) with the trivial $u = 0$ solution. This generates the compactons depicted in figures 1 and 2.

Now, for $u = 1$ to be an admissible solution we need the 'total force' in (15)

$$f \doteq \frac{\lambda}{2}u + F$$

to vanish there. This defines the critical velocity

$$\frac{\lambda_1}{2} = n - m. \tag{18}$$

Turning to equation (17), which is singular at $u = 1$ as well, for $u = 1$ to be admissible as a solution, the potential has also to vanish at this point. This imposes an additional constraint

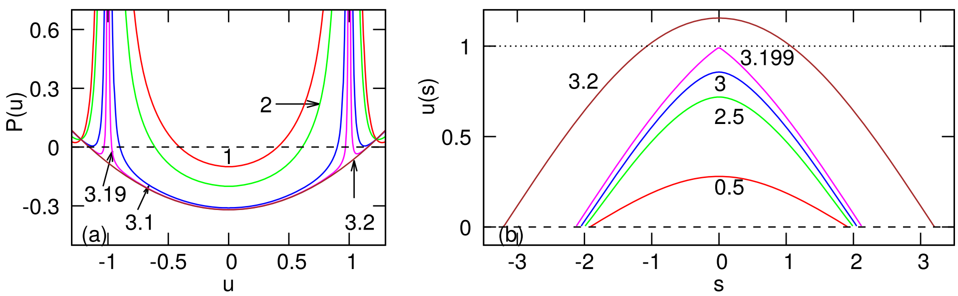

Figure 2. Panel (a): the effective potential $P_{35}(u)/(1-u^2)^2$ for different values of λ ($\lambda = 1$ (red), $\lambda = 2$ (green), $\lambda = 3.1$ (blue), $\lambda = 3.199$ (magenta), $\lambda = 3.2$ (brown)). Note that the effective potential remains finite only at the limiting velocity $\lambda = 16/5$, thus enabling the corresponding solution's trajectory to cross the $u = 1$ level. Panel (b): compacton profiles for $\lambda = 0.5$ (red), $\lambda = 2.5$ (green), $\lambda = 3$ (blue), $\lambda = 3.199$ (magenta), $\lambda = 3.2$ (brown). Note the support of the limiting solution which is much wider than its velocity-wise close neighbours.

on the velocity

$$\frac{\lambda_2}{2} = \frac{(n-m)(m+1)(n+1)}{2nm}. \tag{19}$$

Consistency demands that $\lambda_1 = \lambda_2$, which constrains the admissible powers in $F(u)$:

$$n = \frac{m+1}{m-1}. \tag{20}$$

Thus, since $1 < m < n$, the case $(m, n) = (2, 3)$ emerge as the only pair of integers for which the constraint (20) holds and thus supports formation of solutions incorporating singularities at both $u = 0$ and $u = 1$ (the so-called kovatons [3, 6]).

In fact, since $P^{'} = F'f$ and $P'' = F''f + F'f'$, then at $u = 1$ where $F' = 0$ and $P' = 0$, for P'' to vanish as well, we need that both f and P vanish there with the same velocity. When these conditions are satisfied, u_s vanishes, and both compact kink/anti-kink and $u = 1$ become admissible solutions, which underlines the formation of kovatons (their explicit construction will be provided shortly). Formally,

$$-u_s^2\Big|_{u=1} = \frac{P(u)}{F'^2(u)}\bigg|_{u=1} = \frac{P'(u) = F'f}{2F'F''}\bigg|_{u=1} = \frac{f}{2F''}\bigg|_{u=1}.$$

Since $F'' = -nm(n-m) \neq 0$ at $u = 1$, therefore if both f and P vanish at the same velocity, u_s will vanish as well.

On the other hand, if the potential and the force vanish at $u = 1$ at different speeds, then $u_s \neq 0$, $u = 1$ is not a solution, and kovatons cannot form.

The existence of kovatons may be embedded into a bit more general framework via the invariance of the equations of motion, whether discrete or QC, under

$$u \to 1-u \quad \text{and} \quad F(u) \to -F(1-u) + \text{const.}, \tag{21}$$

or simply into the condition $F'(u) = F'(1-u)$. If F is a polynomial of degree n, one may deduce the constraints for this condition to hold. For $n = 3$ we obtain the G23 model. Among quintic choices the used $F(u)$ in the G35 model provides a counterexample, whereas $F' =$

$u^2(1-u)^2$ supports kovatons. A more general class admitting kovatons is provided by $F' = g(u)g(1-u)$, $g(u=0)=0$, where g may be any smooth function or, by $F = \sin^{2n}(\pi u)$, etc.

3.3. The G23 case

Let $m=2$ and $n=3$. After cancelling of the common u^2 factor, equation (17) reads

$$\frac{3}{2}(1-u)^2u_s^2 + P_{23}(u) = 0, \quad \text{where } P_{23}(u) = -\frac{\lambda}{2}u + \frac{3}{8}(6+\lambda)u^2 - 3u^3 + u^4. \tag{22}$$

For $\lambda < 2$, equation (22) enables one to find numerically the shape of the solitary TW (compacton) and, due to the singularity at $u=0$, to 'glue' the periodic solution at the throw with the trivial state. Several such solutions are displayed in figure 1.

When the amplitude is either large or small, we may derive explicit approximate expressions for the solitary waves. For small amplitudes, neglecting the cubic part in the equation of motion, the resulting compacton takes a simple form

$$u = \frac{2\lambda}{9}\cos^2\left(\frac{\sqrt{6}s}{4}\right) H\left(2\pi - \sqrt{6}|s|\right), \tag{23}$$

where $H(\cdot)$ is the Heaviside function. Invariance under $u \to 1-u$, generates compact drops hanging from the $u=1$ 'ceiling'. Assuming $0 \leqslant v = 1-u$ to be small, we thus have

$$u = 1 - \frac{2\lambda}{9}\cos^2\left(\frac{\sqrt{6}s}{4}\right) H\left(2\pi - \sqrt{6}|s|\right). \tag{24}$$

In the limiting $\lambda = 2$ case, where $P_{23}(1) = P'_{23}(1) = P''_{23}(1) = 0$, the problem simplifies to

$$(1-u)^2\left[3u_s^2 - 2u(1-u)\right] = 0 \quad \text{where } s = x - 2t. \tag{25}$$

Clearly, the singularity at $u=1$ is now accessible and we obtain a kink and/or anti-kink of *a finite span*. Tied together back-to-back they form the basic kovaton (see figure 1)

$$u = \cos^2\left(\frac{s}{\sqrt{6}}\right) H\left(\sqrt{\frac{3}{2}}\pi - |s|\right). \tag{26}$$

Better yet, since $u=1$ is now solution as well, we may insert its segment into the centre and form a combined 'triplet' entity, a flat hat kovaton (see panel (b) of figure 1):

$$u_{\text{kov}}(s) = \begin{cases} A & \text{for } -\sqrt{\frac{3}{2}}\pi \leqslant s + s_0 \leqslant 0, \\ 1 & \text{for } |s| \leqslant s_0, \\ A & \text{for } 0 \leqslant s - s_0 \leqslant \sqrt{\frac{3}{2}}\pi, \end{cases} \tag{27}$$

where $A = \cos^2\left(\frac{s_0-|s|}{\sqrt{6}}\right) H\left(\sqrt{\frac{3}{2}}\pi + s_0 - |s|\right)$ and $0 < s_0$ is an arbitrarily chosen constant, determining the width of the top. Again, due to the invariance of the problem under $u \to 1-u$, we also have an anti-kovaton

$$u_{\text{anti-kov}} = 1 - u_{\text{kov}}. \tag{28}$$

Comparing the basic width of the kovaton (26) with its small amplitude 'sibling' in (23), we notice that the kovaton is $\approx 50\%$ wider. The property that the width grows with the amplitude indicates that the dispersion–convection balance shifts with amplitude toward the dispersion.

For a later use we also record the regime of large amplitude waves, wherein F has already changed its sign and its quadratic part may be ignored, leaving us with only the cubic part. In the resulting problem

$$\frac{\mathrm{d}u_k}{\mathrm{d}t} = 2(u_{k+1}^3 - u_{k-1}^3),$$

the solitary waves propagate to the left ($\lambda < 0$) and their shape is easily derived via the corresponding QC equation

$$u(s) = \pm\left(\frac{3|\lambda|}{8}\right)^{1/2} \cos\left(\sqrt{\frac{2}{3}}s_+\right) H\left(\pi - \sqrt{\frac{8}{3}}|s_+|\right) \quad \text{where } s_+ = x + |\lambda|t. \quad (29)$$

The $\pm$ sign expresses the reduced equation's invariance under $u_k \to -u_k$.

3.4. The G35 case

We now consider the $m = 3$ and $n = 5$ case. Following the reduction by a common factor u^4 in (17), we obtain

$$(1-u^2)^2 u_s^2 + P_{35}(u) = 0 \quad \text{where } P_{35}(u) = -\frac{\lambda}{10}\left(1 - \frac{2}{3}u^2\right) + \frac{2u^2}{3}\left(1 - \frac{3}{5}u^2\right)^2. \quad (30)$$

Its compact solutions are displayed in figure 2. As in the previous case, the singularity at $u = 0$ and the associated local loss of uniqueness enables one to glue the periodic solution with the trivial state to form a compacton which, though continuous, has a jump at $u = 0$ in its first derivative.

As in the other case, for small amplitudes one keeps only the lower order part in $F(u)$ with the explicit form of compactons, up to a normalization, given via (29). In the opposite case of large amplitudes solitary waves, keeping only the quintic part, we have

$$u(s) = \pm\left(\frac{5|\lambda|}{18}\right)^{1/4} \cos^{1/2}\left(\frac{2\sqrt{6}}{5}s_+\right) H(2\pi\sqrt{6} - 10|s_+|) \quad \text{where } s_+ = x + |\lambda|t. \quad (31)$$

As in (29), the resulting compactons propagate to left, $\lambda < 0$.

We now turn to address the behaviour near the $u = 1$ singularity. From (30) we have $P_{35}(u = 1) = (16/5 - \lambda)/30$. At the critical velocity $\lambda = 16/5$, $P_{35}(1) = P'_{35}(1) = 0$ (since $f \neq 0$, $P''_{35}(1) \neq 0$). At the limiting velocity we thus have

$$(1-u^2)^2\left[25u_s^2 - 6\left(\frac{4}{3} - u^2\right)\right] = 0 \quad \text{where } s = x - \frac{16}{5}t. \quad (32)$$

Though in the present case *kovatons cannot form*, at the limiting velocity, *and only at this velocity*, the singularity at $u = 1$ allows the regular solution trajectory to 'sneak through' and cross it (in $u = 1$ vicinity $u \sim 1 + as + bs^2 + \ldots$ where $a = \frac{\pm 1}{5\sqrt{3}}$ and b is a constant) and the limiting solution takes a simple form

$$u(x,0) = \frac{2}{\sqrt{3}}\cos\left(\frac{\sqrt{6}x}{5}\right) H\left(5\pi - 2\sqrt{6}|x|\right). \quad (33)$$

Notably, in addition to this exceptional solution, the singularity at $u = 1$ admits also a solution which is non-smooth at its top

$$u(x, 0) = \frac{2}{\sqrt{3}} \cos\left(\frac{\pi}{6} + \frac{\sqrt{6}|x|}{5}\right) H\left(5\pi - 3\sqrt{6}|x|\right), \tag{34}$$

attained at $u = 1$ and is thus a *compact peakon*: it has a finite support, is everywhere continuous, but its first derivative at the peak switches its sign $\pm 1/\sqrt{3}$. From figure 2 one also notes that whereas the support of the exceptional solution undergoes a sizeable jump with respect the support of its speed-wise close neighbours, the support of the peakon solution is a continuous extension of the support of its velocity-wise close neighbours and may thus be considered as their natural extension.

3.5. The relevance of quasi-continuum based analysis

Before leaving the QC realm we need to clarify the role of the QC in elucidating the discrete patterns, but first some basic facts. Whereas the singularity at $u = 1$ bounds the domain accessible by the PDEs, as we shall shortly see, the discrete antecedents have no such barrier and at $u = 1$ there is merely a 'road sign' of things to change. In fact, both the G23 and the G35 discrete problems have large amplitude solutions which are far beyond the access of their respective QC PDEs representations. Yet though those PDEs failed to cross the $u = 1$ barrier, the QC approach may be still of use if applied separately to the small and large amplitude domains, see equation (9) and solutions (23), (29) and (31). This is not a contradiction because *the singularity is a barrier of the PDEs and not of the original problem*. We may bypass the 'barrier' at $u = 1$ by splitting the PDE representation into a 'sub-critical' domain, valid up to the singularity, and a 'super-critical' QC description, applied at large amplitudes, equation (9), where both F and F' have already changed their signs, with the corresponding large amplitude solitary solutions recorded in (29) and (31), respectively.

And yet, though the discrete problems appear formally to be oblivious of the singular barriers, nonetheless those barriers appear to be somehow implicitly imprinted in the system (similar phenomenon was also observed in [5]). We shall find again and again that the more interesting action in the discrete realm takes place in a close vicinity of those singular transitions unfolded by PDEs which per se are no longer valid there!

Existence of a thin layer where *the discrete effects are essential*, is analogous to the emergence of shock waves in an ideal gas in a boundary layer. There, whenever the Euler equations break down, one has to restore the viscosity, or better yet, to evoke the original gas-kinetic description. Yet away from the breakdown zone, the Euler equations work well. Notably, in both gas dynamics and in our problem, the more complex and intriguing phenomena occur in the transition zone, marked by the ideal PDEs, yet described only via the original kinetic or the discrete setup to be unfolded next.

4. Basic travelling waves, TWs, on a lattice

4.1. Integral formulation

Returning to the original discrete problem, we seek solitary travelling waves on the lattice (1) of the standard form

$$u_k(t) = U(t - ka) \quad \text{where } a = 1/\lambda.$$

Substitution in (1) yields a delayed-advanced equation

$$\frac{dU}{dt} = F[U(t-a)] - F[U(t+a)].$$

Assuming that $U(\pm\infty) = 0$, we integrate the last equation and set $t = as$ to simplify the resulting nonlinear integral equation

$$\lambda U(s) + \int_{-1}^{1} F[U(s+s')]ds' = 0, \tag{35}$$

which will be explored next.

4.2. The Newton–Raphson algorithm and linear stability analysis

Equation (35) is in a form which enables application of the Newton–Raphson algorithm using the standard continuation approach [30]. The free parameter λ was used to search for branches of solutions. Assuming a given (λ_0, U_0) solution, to find a new one we append equation (35) with an auxiliary equation

$$(\lambda - \lambda_0)^2 + (N[U] - N[U_0])^2 = \Delta^2, \quad \text{where } N[U] = \int U(s)ds$$

is the integral of the solution, and Δ a (small) shift parameter. A solution pair (λ, U) of the extended system is then sought via the Newton–Raphson algorithm. In practice, we have used $\Delta = 10^{-2} - 10^{-4}$, and the integral in (35) was evaluated using the Simpson formula, with a typical step of $\Delta s = 0.02$. Solving the joint system for $U(s)$ and λ we advance along the solutions branch. Since the TW tails decay at a doubly-exponential rate [2, 6, 8], for all practical purposes their span may be considered finite. Therefore in choosing the integration domain we take $|s| \leqslant L$; with L assumed to be an integer and chosen such that $|U(L-1)| < 10^{-16}$ (if this condition was violated, the range was extended to $L \to L+1$).

Once a solution was found (only symmetric solutions, $U(-s) = U(s)$, were explored), its stability was tested. Since it is difficult to explore stability of travelling waves on an infinite lattice, we have exploited the strong localization of solutions and examined them on a finite size, l, lattice appended with periodic boundary conditions. The resulting travelling wave is a periodic orbit of a finite-dimensional system having a period l/λ. We have constructed numerically the corresponding monodromy matrix and found its eigenvalues—the characteristic multipliers of the periodic orbit. A stable solution has all its multipliers on a unit circle, whereas the instability may be detected by calculating the logarithm of the absolute values of the multipliers. To enhance our confidence in the derived results, we have also examined stability via a direct numerical simulation of the original lattice equations on a small lattice. Both methods yielded the same results.

4.3. Basic TW branches in the G23 model

In figure 3 we present the branches of the TWs found in the G23 lattice (4). Their features may be summarized as follows:

- There is a branch of solutions which is very well described by the QC, section 3.3 (marked with brown crosses in figure 3). The displayed solutions are noted at lettered points (d), (e) and (f) in figure 4. *All waves along this branch are stable.* For small amplitudes equation (4) may be approximated via (9) with $\alpha = 3$. Being at this regime invariant under $u \to -u$, $t \to -t$, implies that small-amplitude compactons are nearly symmetric.

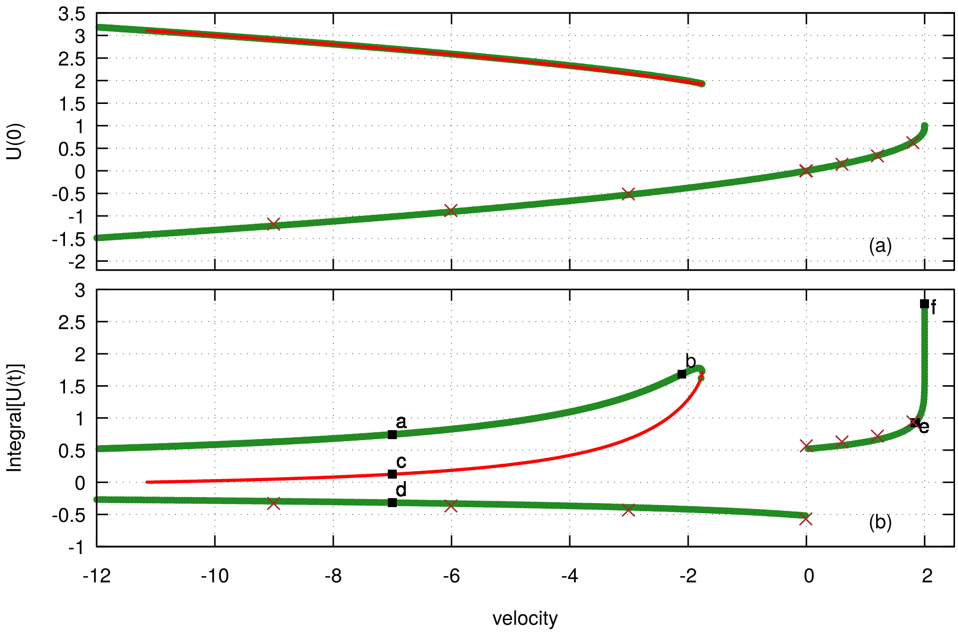

Figure 3. Basic travelling wave branches in the G23 model, equation (4). Panel (a): the field at the centre $t = 0$ vs velocity; panel (b): the integral of the profile vs velocity. Solutions at marked points are depicted in figure 4. Green bold lines: stable waves, red thin line: unstable waves. Brown crosses: values predicted by the QC theory. Note the green colour which hides behind the red in the upper branch of the panel (a) and the solutions a and c which have the same amplitude and velocity, but different integrals (masses). Though we have depicted the branches only in a finite range of parameters, there is an ample numerical evidence to assume that these branches could be prolonged *ad infinitum*.

- At large amplitudes wherein $F(u)$ has already changed its sign, the unfolded branch has *negative velocities.* Equation (29) may be viewed as its QC representation. This branch relies on $F(u)$ being positive and cannot be extended to small amplitudes/velocities. The patterns corresponding to lettered points (a), (b) and (c) are depicted in figure 4. Notably, only waves with a larger integral are stable (in the upper amplitude–velocity diagram (panel (a)) the stable and the unstable branches nearly overlap, a much clearer distinction between these branches is provided by the integral-velocity panel (b)). Note also that on the presented large amplitude branch, the quadratic part of F though small is not completely negligible, which affects the proximity between the analytical and the numerical results. It may also affect the stability of a wave, for unless the pulse is truly large, for a sizeable part of its profile $F(u)$ is positive with this part's tendency to propagate to the right. Values of u have to be considerably over $F's$ transition value $3/2$ for the dynamics to enforce a stable propagation to the left.

4.4. Basic TW branches in the G35 model

We now address the basic solitary TW in the G35 model (5). Due to the $u \to -u$ symmetry, it suffices to display in figures 5 and 6 only waves with positive amplitudes, and to skip their

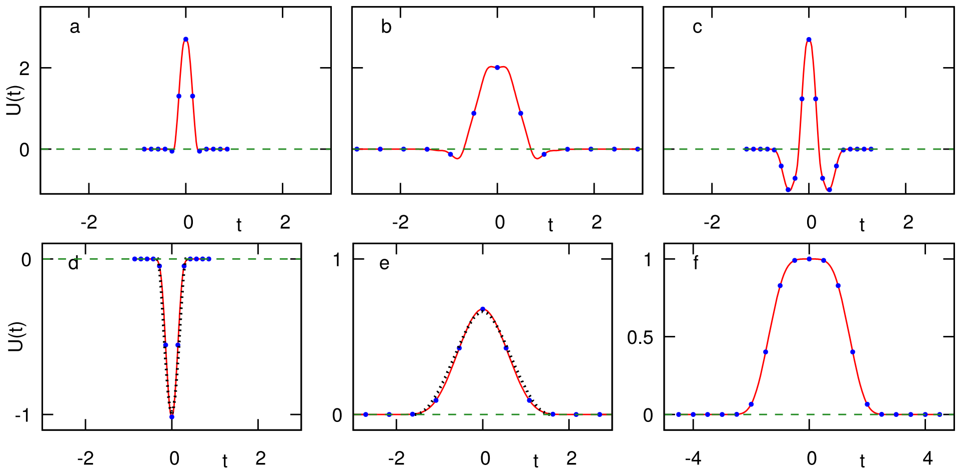

Figure 4. Basic travelling waves profiles $U(t)$ at the corresponding lettered points on the diagram in figure 3. Red lines: profiles as function of time. Blue circles: snapshots on the lattice. Note that TW velocity in cases (a), (c) and (d) is the same, though with case (c) being unstable, see figure 3, one may not be able to observe its propagation. In panels (d) and (e) we also display with black dotted lines the profiles of the QC representation for the same λ.

symmetric negative amplitude counterparts. For the unfolded solitary waves we have found that:

- As in the G23 case, the G35 small amplitudes regime is very well described by the QC (section 3.4). However, at larger amplitudes as one approaches the transition zone the features of the found waves diverge considerably from their QC representation. To recall, the QC yields a continuous branch of solutions with amplitudes ranging from zero to one and the corresponding velocities in the $[0, 16/5]$ range, with one exceptional solution which attains the maximal velocity $16/5$ and the maximal amplitude $2/\sqrt{3}$ and a much wider support. However, unlike the QC, the solution branch of the discrete antecedent bridges continuously between the disconnected QC solutions (see panels (d) and (e) in figure 6). Furthermore, we also find an entire branch of discrete solutions, of which the QC is completely oblivious, with amplitudes hovering slightly below the exceptional QC amplitude $2/\sqrt{3}$ and the velocity $16/5$, with widths which may be chosen at will (see panel (f) in figure 6). An enlarged display of the layer in the vicinity of point (e) in figure 5 is shown in figure 10. Clearly, in this layer there is a very strong interaction between the nonlinearity and the discreteness which has an essential impact on the resulting dynamics which the QC does not seem to be able to reproduce. Moreover, whereas in the G23 model both the discrete problem and its QC representation yield kovatons residing on the singular manifold, as a flat-top solutions of arbitrary width, the presented almost flat-top solutions on the G35 lattice (though they appear to be *unstable*), occur only in the discrete model. Notably, their amplitude is close to $2/\sqrt{3}$, the maximal QC amplitude and their speed to a high accuracy is $25/8$, i.e. slightly below the maximal QC speed.

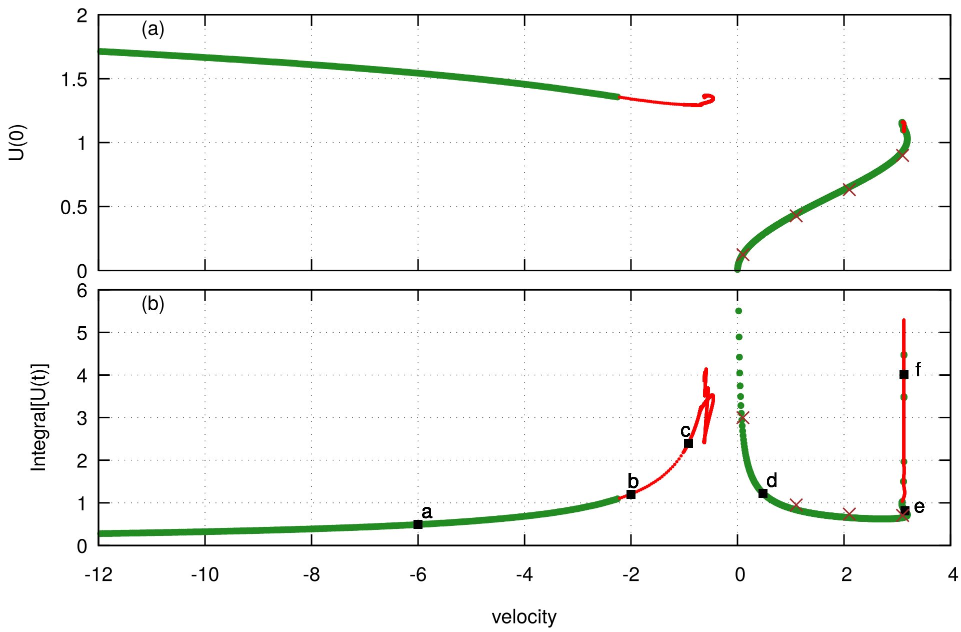

Figure 5. The basic TW branches in the G35 model, equation (5). Panel (a): the field at $t = 0$ vs velocity; panel (b): the integral of the profile vs velocity. Green bold lines and circles: stable TWs, red thin lines: unstable TWs. Solutions at marked points are depicted in figure 6. Brown crosses show the corresponding values of TW in the QC representation. The upper panel clearly shows an amplitude gap which may cause TW located close to the right edge of the left branch to 'hop' to the right branch, with a consequent switch of direction, whether due to inner instability or collision, if the resulting amplitude falls below the minimal admissible value of the left branch. Such scenarios are displayed on figures 13 and 14. Figure 15 shows a reverse scenario: collision between waves on the right branch causes one wave to hop to the left branch and then hop back. Although depending on the direction of hopping, the amplitudes of waves may increase or decrease, their masses hardly change. Though we have depicted the branches only in a finite range of parameters, there is an ample numerical evidence to assume that the branches could be prolonged *ad infinitum*. To demonstrate this feature we zoom up the vicinity of marker 'c' and display it in figure 7.

- As before, at large amplitudes one finds another branch of discrete solutions (figure 6, panels (a), (b) and (c)) which may be approximated by the large amplitude QC solutions (31). We have then extended these solutions to smaller amplitudes/velocities where they start to resemble multi-oscillatory wave packets. Figure 7 focuses on this part of the bifurcation diagram. Presumably, extending this branch will yield solutions which are ever more oscillatory.
- Similarly to the G23 case one notes the almost inverse relations between the integral (which up to a sign is the mass of the wave) and the sensitivity of the amplitude to the changes in the wave velocity. This comes out in figures 13–16, where we display waves hopping from one branch to the other. The jump from right (left) branch to the left (right) results in amplitude increase (decrease), but as figure 5 clearly shows, hardly in any changes in its integral.

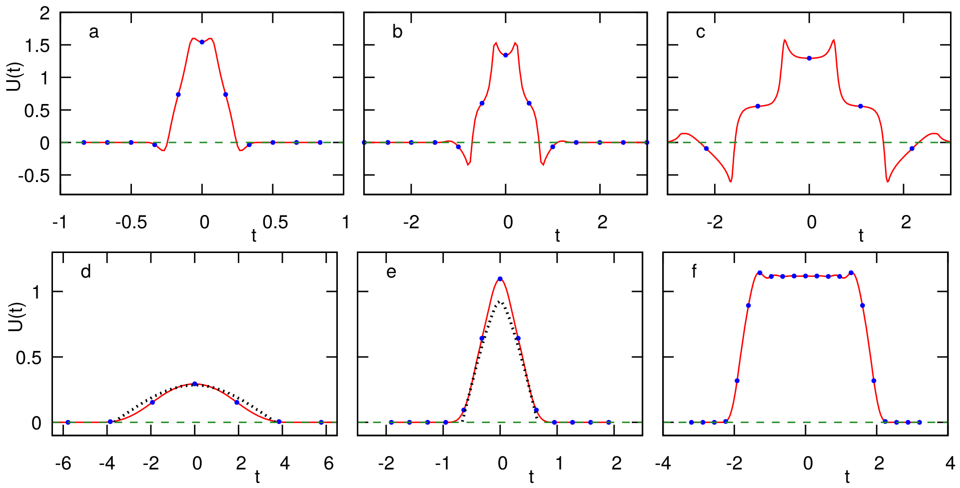

Figure 6. Display of the basic G35 TWs located at the corresponding lettered points in figure 5. Red lines: amplitude as a function of time. Blue circles: amplitude snapshots on the lattice. Surprisingly enough the amplitude of the flat-like case (f) is not $\sqrt{5/3}$ where $F(u)$ vanishes, but much closer to $2/\sqrt{3}$, the amplitude of the only QC compacton solution, see figure 2, that sneaks through the $u = 1$ barrier, though its velocity $25/8$ is slightly under the maximal QC speed $16/5$. In panels (d) and (e) we also display in black dotted lines the corresponding profiles obtained via the QC representation.

5. Interlaced travelling waves, ITW

We now proceed to unfold a more evolved class of solitary travelling waves which have distinct profiles at odd and even sites and appear as two interlaced solitary waves. They may be considered as a simple form of moving breathers, and will be referred to as interlaced travelling waves, ITWs. Denoting

$$u_{2k}(t) = U\left(t - \frac{2k}{2\lambda}\right), \qquad u_{2k+1}(t) = V\left(t - \frac{2k+1}{2\lambda}\right),$$

gives a system of two coupled equations

$$\frac{\mathrm{d}U}{\mathrm{d}t} = F[V(t-\lambda^{-1})] - F[V(t+\lambda^{-1})],$$
$$\frac{\mathrm{d}V}{\mathrm{d}t} = F(U(t-\lambda^{-1})) - F[U(t+\lambda^{-1})].$$

Setting $t = \lambda^{-1}s$ and following the same procedure as in section 4.1, yields a system of two coupled integral equations

$$\begin{aligned} &\lambda U(s) + \int_{-1}^{1} F[V(s+s')]\mathrm{d}s' = 0, \\ &\lambda V(s) + \int_{-1}^{1} F[U(s+s')]\mathrm{d}s' = 0. \end{aligned} \tag{36}$$

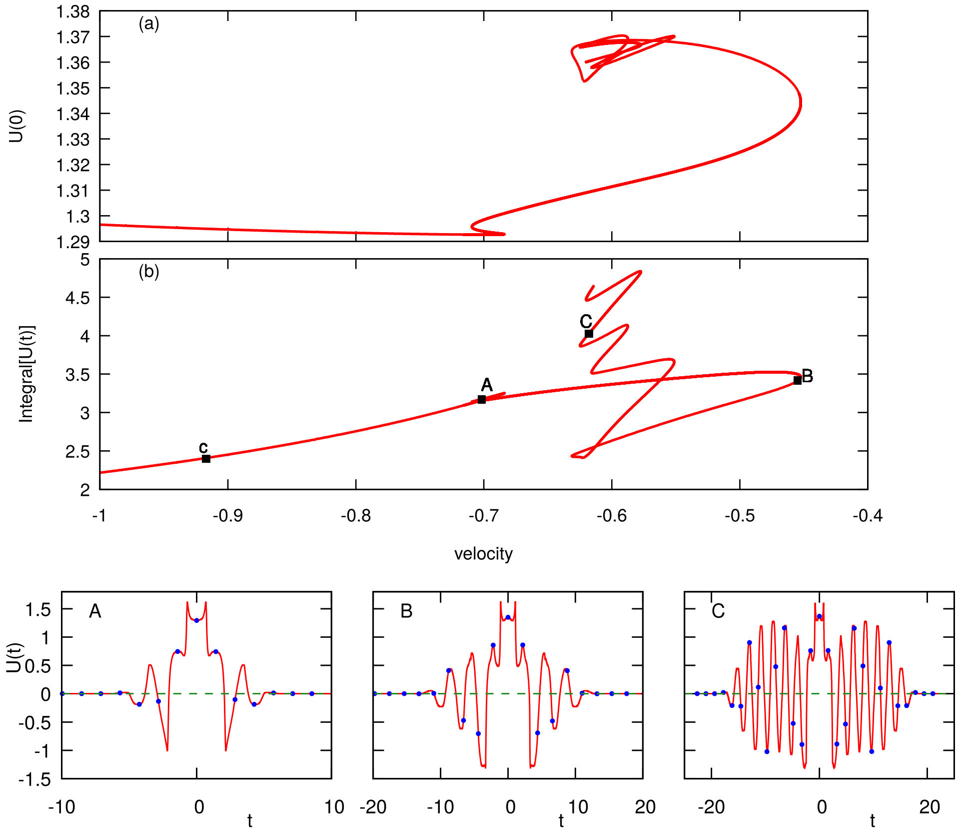

Figure 7. Panels (a) and (b): a magnified part of the diagram in figure 5 for small negative velocities; notations as in figure 5. Bottom panels (A)–(C): profiles of solutions at marked places on the diagram; notations as in figure 6. Note that whereas the central part of the solutions is nearly the same, their oscillating tails expand, presumably ad infinitum. Marker ‘c’ on the left in panel (b) is at the same location as in figure 5 above.

5.1. Staggered compactons

In systems with an $F(-x) = -F(x)$ symmetry, a simple interlaced solution may be derived from the basic TW. Setting $V = -U$ reduces system (36) into one equation

$$(-\lambda)U(s) + \int_{-1}^{1} F[U(s+s')]\mathrm{d}s' = 0,$$

which coincides with (35). Thus any basic TW in a symmetric system produces an ITW with an opposite velocity. Because the profiles at the odd and even sites are equal and opposite in sign, we shall refer to such wave as a ‘staggered compacton’ in analogy with staggered solitons, cf [31].

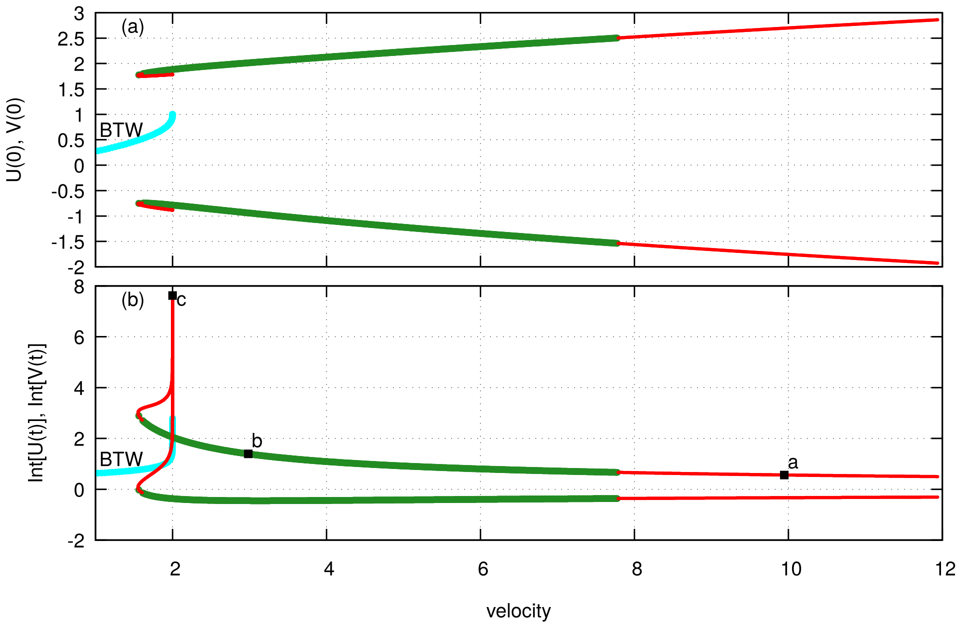

Figure 8. Branches of the ITW in the G23 model (4). Green bold lines: stable waves, red thin lines: unstable waves. The basic TW branch is also shown (in cyan, it is also marked as BTW to be distinguishable in a black and white form). Though we have depicted the branches only in a finite range of parameters, there is ample numerical evidence that these branches could be prolonged *ad infinitum*.

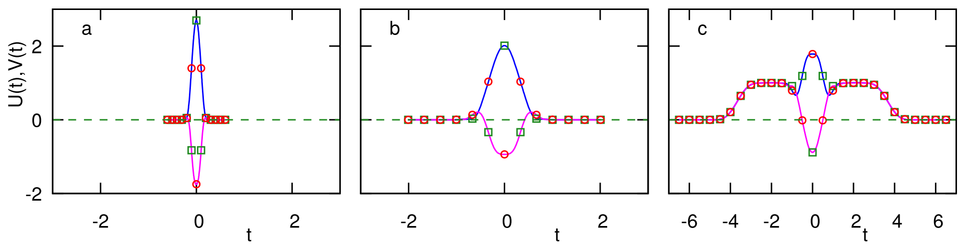

Figure 9. Display of the G23 ITWs at the corresponding lettered points on the diagram in figure 8. Blue and magenta lines: profiles at even and odd sites as functions of the time. Green squares and red circles: snapshots on the lattice (when the centre passes even and odd sites). Note the more intriguing patterns in *a* and *c* which emerge in the vicinity of the QC critical speed.

5.2. Interlaced travelling waves, ITW

Applying the same numerical procedure, including analysis of stability, similarly to the basic TW case, we now proceed to unfold the less obvious branches of the interlaced travelling waves,

The G23 model. Figures 8 and 9 display the ITWs in the G23 lattice. Our understanding of these waves is based on their large amplitude domain wherein the waves have negative velocities (thus propagate to the left) residing on a corresponding branch in figure 3. In

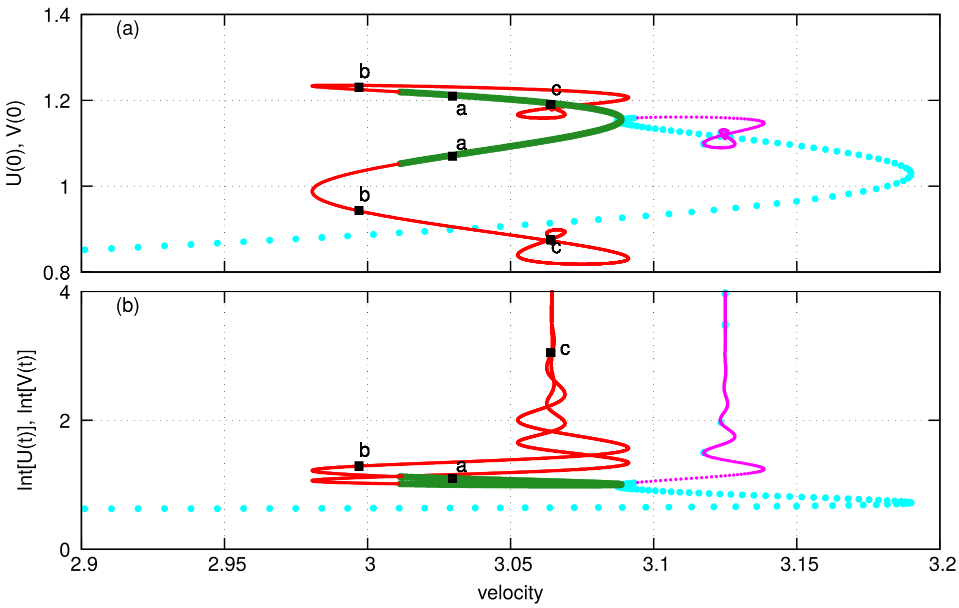

Figure 10. The interlaced TW branches of the G35 model. Note that the main action takes place in the vicinity of the critical transition. Green bold lines: stable waves, red thin lines: unstable waves. The presented waves do not seem to be related to the symmetrically staggered compactons for, unlike the G23 model, the amplitudes of U and V, being both are positive, are far from being reflection of each other, see figure 11. The basic TW branch is also displayed for comparison (stable TWs with large filled circles in cyan, unstable TWs with small circles in magenta).

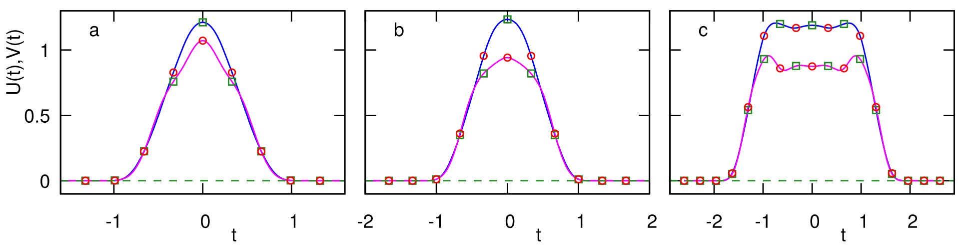

Figure 11. Profiles of the interlaced TW corresponding to the lettered points in figure 10. Blue and magenta lines: profiles at even and odd sites, respectively, as functions of the time. Green squares and red circles: snapshots on the lattice (when wave's centre passes the even and the odd sites).

addition, since at large amplitudes the system is anti-symmetric in u, in this limit it also supports staggered compactons which propagate to the right. This corresponds to the ITW solution in figure 8, where at large positive velocities the solutions are seen to be nearly staggered (panel (a) in figure 9). At smaller velocities/amplitudes, return of the quadratic part in $F(u)$ to the game ruins the symmetry between odd and even sites (panel (b) in figure 9). Formally, since the staggering ansatz leaves the $(-1)^k$ factor in front of the quadratic part, its sign and thus its impact changes with the parity of k, causing the resulting amplitudes of odd and even sites to be different. Notably, this branch of solutions extends to velocities slightly under 2, where

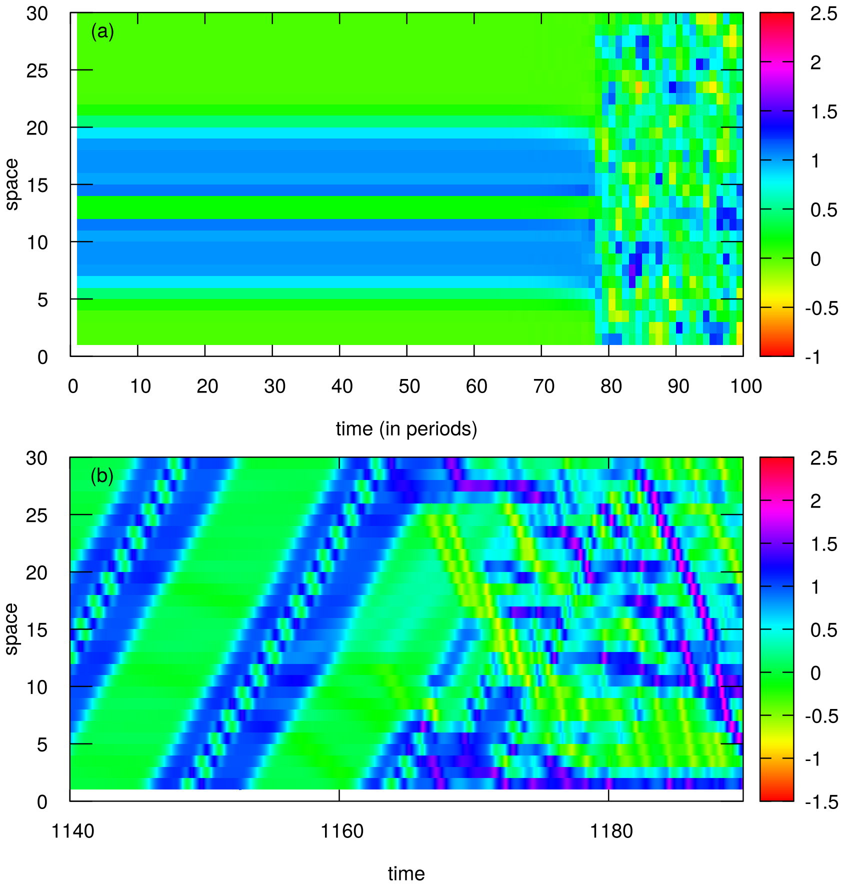

Figure 12. G23 lattice. Space–time diagram of the evolution of an interlaced TW (case (c) in figure 9). It preserves its shape for about 75 periods (about 2250 sites). Panel (a) shows the stroboscopic (with a period equal to travelling time on a lattice of length 30) frames, and in this representation the moving travelling wave looks like a steady-state solution. Panel (b) which has 30×10^4 'pixels' shows the last stage of travelling wave's existence and its subsequent disordered decomposition.

it co-exists with the basic TW branch, also depicted in figure 8. There seems to be some sort of 'resonance' between these waves which induces large-integral solutions at a velocity of ≈ 2, with the resulting pattern having a remarkable flat-like appearance with a quasi-staggered compacton riding on its top (panel c in figure 9).

The G35 model. Figures 10 and 11 display the branches of the ITWs in the G35 lattice. The first thing to note is that the whole action takes place in a strip close to the critical speed $16/5$, where $F(u)$ is still positive. As already aforementioned few times, in this domain the discrete effects play an essential role. However, this ITW branch does not appear to be a staggered version of the basic TW. Instead, it seems to be a result of a certain symmetry-breaking in (36). At its tip, this branch touches the basic TW's branch. Close to the tip the profiles at even and odd sites appear to be similar (panel (a) in figure 11). Along the ITW branch the difference between the even and odd sites profiles increases, but never becomes large: they look like mirror cases of the flat-top solitons; one amplitude is above 1 whereas the other under it (panels (b)

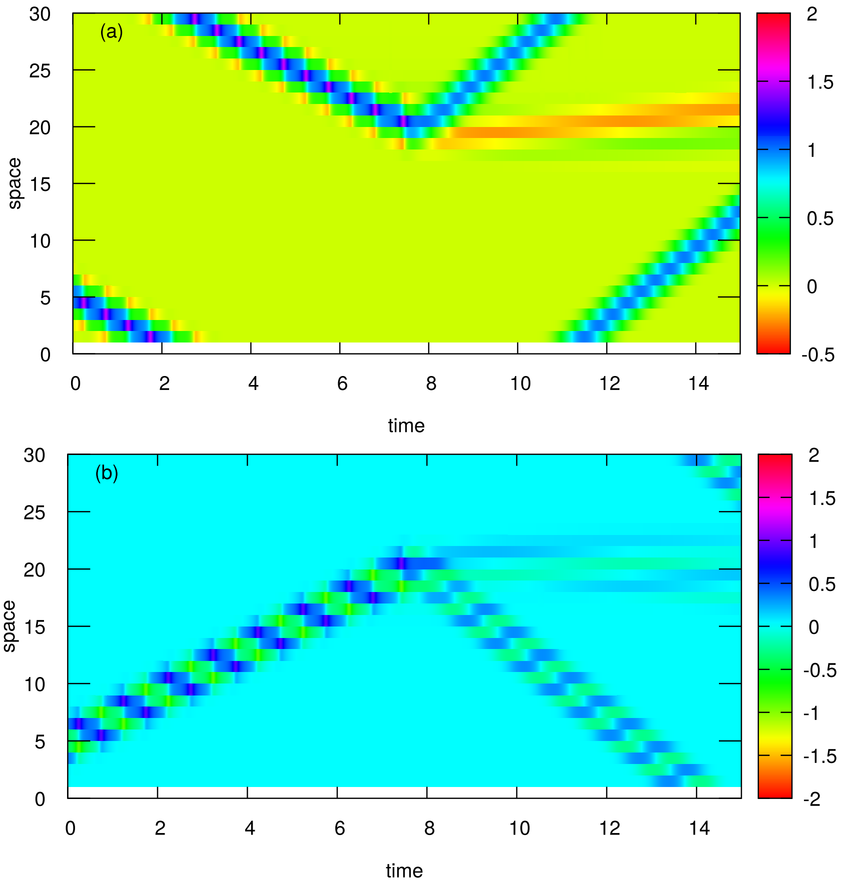

Figure 13. Reversal of soliton's path in the G35 model. Top panel: space–time diagram of a weakly unstable TW to the left. Due to its instability and proximity to branch's edge, when wave's amplitude becomes too low to be sustained by the left branch, it hops to the other branch with a corresponding change of propagation direction. The lower panel displays the corresponding scenario for its staggered twin with its propagation in the opposite direction. Each diagram consists of 30×5000 'pixels'.

and (c) in figure 11). Though it is tempting to relate the last pair with the basic TW in figure 6, the later attains a higher velocity on the threshold of the critical speed.

Finally, we note that due to the anti-symmetry of the G35 lattice, any interlaced solution (U, V, λ), like the ones in figures 10 and 11, always has an associated staggered counterpart $(U, -V, -\lambda)$.

6. Direct numerical simulations

In the numerical simulations of the lattice (3) all the unfolded TW can be easily observed: stable waves exist on an extremely long time intervals, unstable solution gets eventually destroyed. Though most of the unstable TWs decompose within few time units, in direct numerical simulations of the interlaced TW of the G23 model (figure 8), several weakly unstable waves persisted

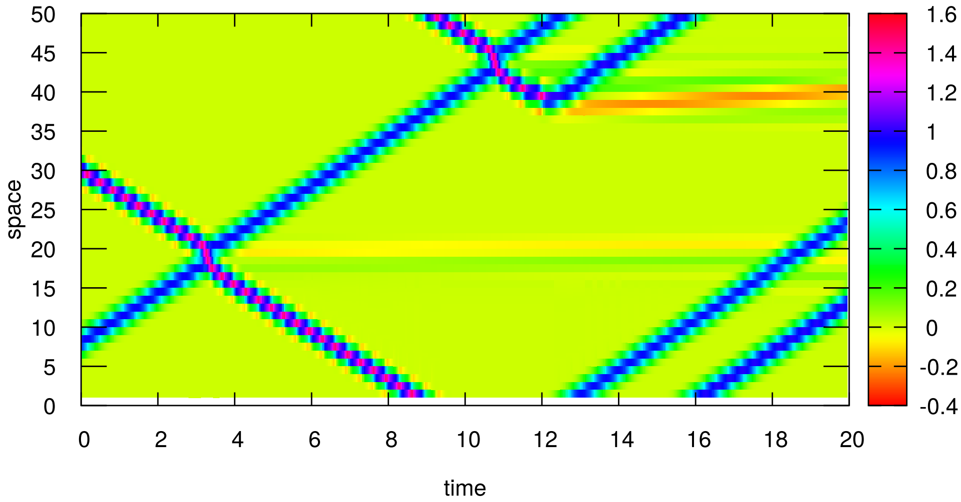

Figure 14. Collisions of a left-propagating (with amplitude 1.4024) and right-propagating (amplitude 1.097) solitary waves in the G35 periodic lattice of length $N = 50$. After two collisions the left-propagating wave reverses its direction resulting in two right-propagating waves and some debris due to the collisions.

for a long time. For instance, a wave with the maximal velocity of $\lambda \approx 12$ decomposes only after $t \approx 400$ (i.e. traversing for about 4800 sites while preserving its shape).

The ITWs on the left side of the diagram in figure 8, with velocity $\lambda = 2$ and large integrals, are also relatively stable or, differently stated, only weakly unstable. This is demonstrated in figure 12, where the waveform (displayed on a lattice of size 30 at each period of revolution, $30/\lambda = 15$) remains intact for at least 75 revolution periods (i.e. up to $t \approx 1150$). We stress here, that in all space–time plots below we display the field on a lattice and thus no 'smoothness' is expected in the space coordinate. The discreteness of the spatial coordinate makes the resulting drawings appear as being of 'poor quality', but this is in earnest an intrinsic feature of the spatio-temporal representation of solutions of lattice equations. The space–time plots in figures 12–16 should therefore be interpreted as collections of N horizontal stripes, where N is the length of the lattice.

We emphasize here, that in all explored cases, an instability of a travelling wave lead ultimately to a disordered (chaotic) pattern (cf figure 12), or to a travelling wave from another branch (cf figure 13). Close to a stability threshold, we have never encountered a stable regime close to the found basic travelling wave solution.

6.1. Reversal in propagation direction

A far more intriguing manifestation of the weak instability emerges in numerical simulations of TWs in the G35 lattice (figure 5), where we have noticed that a weakly unstable left-propagating wave, $\lambda = -2.004\,67$, see figure 13(a), after propagating for about 8 time units, comes to a halt, wobbles for a while, and then *reverses its direction and turns into a stable right-propagating TW*. The same phenomenon is observed in the corresponding staggered case (see figure 13(b)).

The key to the understanding of the reversal of the direction is implicitly embedded in figure 5 with its two panels complimenting each other. The upper panel displays an amplitude/velocity gap between the two branches wherein no propagation is admissible, with the

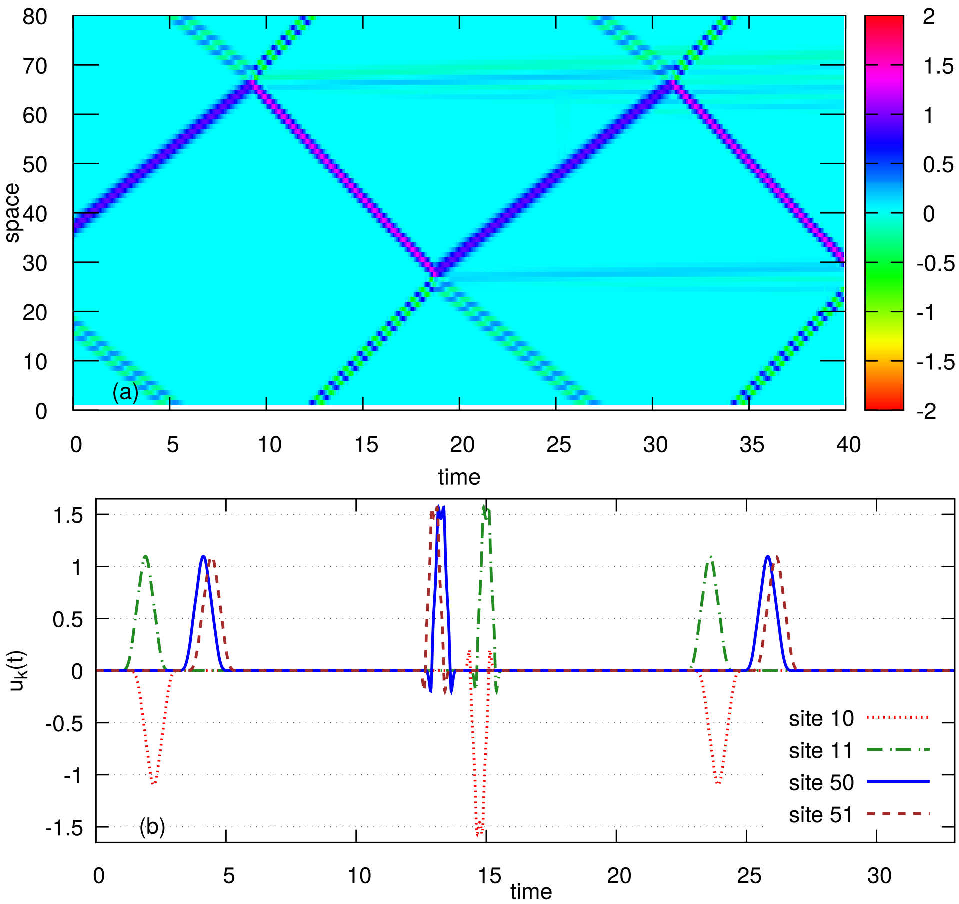

Figure 15. G35 periodic lattice of length $N = 80$. Collisions of a right-propagating wave (with amplitude 1.097) with its staggered twin. (Note that the dynamics depends crucially on the initial distance between the two waves. Shift by one lattice site shown in figure 16 results in a very different dynamics). On panel (a), a collision at $t \approx 10$ transforms the right moving wave into a left-propagating wave on the left branch. With an opposite effect on its staggered twin. The next collision at $t \approx 20$ brings them back to their original branch. To visualize the 'bouncing' impact on waves shape, we display in panel (b) time series at two neighbouring points pairs; $k = 10$ (red dotted line) with $k = 11$ (green dash-dotted line) and $k = 50$ (blue solid line) with $k = 51$ (brown dashed line). The red and green profiles at neighbouring sites $k = 10, 11$ have opposite signs; consistent with the staggered nature of the wave, whereas the blue and brown profiles at sites $k = 50, 51$, being merely shifted, indicate a basic travelling wave. The chosen times cluster prior to the first, the second and the third collision. Though each encounter is accompanied by amplitude change—the mass (integral) itself hardly changes.

waves propagating in opposite directions on each side of the gap. However, the lower panel reveals that the amplitude/velocity jump is a non-event from the integral point of view, for the integral hardly changes after the event (note the almost opposite amplitude–velocity and integral-velocity relations). The jump merely reshapes the wave's profile, and thus its amplitude, with the resulting direction of propagation being a *consequence of the branch on which it has landed.*

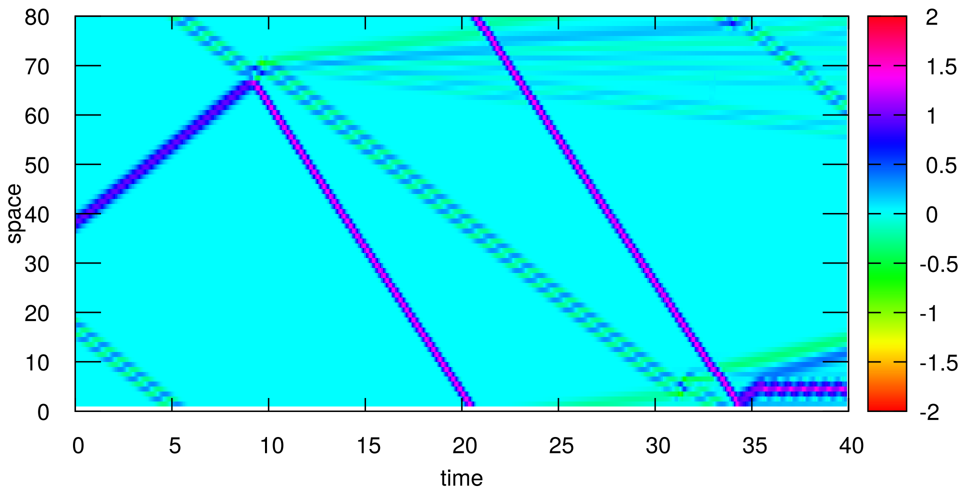

Figure 16. Set-up similar to figure 15, but with the initial separation between the waves shifted by one site. Now after one collision the right-propagating wave turns into a fast left-propagating wave, but its staggered (left-propagating) twin stays the course and turns into another left-propagating staggered wave.

With this understanding we may readily follow figure 14 where the two collisions between the right and the left moving waves suffices to relegate the left-moving wave into the other branch. Figure 15 is a natural continuation of this scenario: here we have a back and forth bouncing between the opposite branches, starting from the right branch on figure 5 and being pushed after one collision to the other branch. Following the second collision both waves are back at their original, right, branch and the game continues. This could have gone indefinitely would it not be for the fact that the collisions are not entirely elastic with some debris created after each event.

Unfortunately, as figure 16 attests, the interaction *is very sensitive* to the collision phase of the TW and its staggered twin. A shift by merely one lattice site in the initial position of one of the waves causes the bouncing effect to disappear.

In the G23 model, things are much simpler; no reversal of direction was ever observed. A weakly unstable TW located close to the right edge of the left branch, propagates for a while but then decomposes into disordered pieces with no observable coherent structure.

7. Summary and closing comments

In the presented paper we have studied the travelling patterns of our strongly nonlinear lattice versions of the Gardner-like model equations G23 and G35, equations (4) and (5), respectively. Three distinctive classes of travelling and non-travelling solitary patterns were unfolded:

(a) Basic travelling waves,TW.
(b) Interlaced travelling waves, ITW.
(c) Stationary solitary states.

Of the three classes, the second and the third have no quasi-continuum, QC, counterpart, which is to say that space-wise these are essentially discrete phenomena, unlike the first class which in part was very well replicated via the quasi-continuum. Yet in spite of what may seem as a limited success of the QC, it did play a vital role in delineating the road map without which most of the first and the second class solutions would not have been unfolded. To be clear, we stress that we do not claim that all TW and ITW were found. In fact, since our method relies on the Newton-Raphson procedure, a good initial approximation is vital, and to this end we have used direct numerical simulations to generate the initial approximation. Therefore, we could unfold only solution branches which have at least one stable segment, leaving the completely unstable branches beyond our reach. Moreover, we can say nothing about the potential existence of other solutions apart the ones presented.

The utility of the QC extends well beyond its direct applicability, for though formally the original discrete system seems oblivious of the singularities, a hallmark of the QC, it appears that those singular manifolds are somehow implicitly embedded in the system and both control and determine the crucial transition zone, in spite the fact that the underlying PDEs are not valid there. Consider, for instance, figures 3 and 8 of the G23 model and figures 5 and 10 of G35 model, respectively. The role of the critical velocity $\lambda = 2$ which emerges in the QC is clearly seen in figure 3, but its role is even more significant in figure 8. This figure describes the quintessentially discrete ITWs, for though there is no corresponding QC counterpart (and thus there are unrelated to the breathers found in the original Gardner equation), yet the most interesting phenomena cluster around the critical values. The same effect is seen in the G35 model with $\lambda = 16/5$ emerging from the QC as the critical velocity. Besides its role as the edge of a 'QC' branch in figure 5, the more impressive scenario is reserved for figure 10, where all ITWs cluster in a narrow velocities strip located just under the critical velocity, whereas in the G23 model the ITWs in figure 8 surround the critical $\lambda = 2$ line from both sides, with a respective zoo of patterns, see figure 11. All in all, we have obtained an amalgam of essentially discrete patterns concentrated around the macro constrains set by the QC.

As a motivation for the present work we have stated that the polynomial force was adopted because of the difficulty to treat the periodic cases. Indeed, we were greatly helped by the existence of large amplitude regimes in the polynomial cases which enabled us to unfold both new branches and new types of waves. Unfortunately, in the original periodic cases there are no large amplitude regimes and with everything being eternally coupled, the presented results seem to provide only a limited help.

It might be of some interest to compare the compactons in the Gardner-type strongly nonlinear lattices explored in this paper with those emerging in the Hertzian version of FPU [1, 2, 14–18] and other similar fully-nonlinear models [4, 5, 8]. Apart from the obvious difference that one is of first order in time whereas the other of second order, the fundamental difference is in the nature of their underlying potential: in the Gardner lattice the potential is non-convex, and in the cited explorations of fully-nonlinear lattices as a rule only a convex potential was used. The riches of our model are due to this non-convexity. Indeed, in the Gardner-type lattices only the small amplitudes compactons, where the non-convexity does not yet play a role (see, for example, the solutions depicted in figures 6(d) and 4(d) and (e)), are close in form to the corresponding solutions of the Hertz-type and other monotone stress lattices. A plethora of the phenomena unfolded in the present work, like the existence of critical amplitudes at which kovatons and peakons emerge, the oscillating compacton profiles, the existence of branches of compactons, or of interlaced travelling waves, relies essentially on the non-monotonicity of the nonlinearity and therefore cannot occur in the Hertzian lattices, or for that matter in any Newtonian-like systems endowed with a convex stress.

The closing comments are reserved for the discrete stationary solutions briefly outlined in section 2. They span a finite plateau defined by the roots of $F(u) = 0$ and initially vanish elsewhere (unlike the TWs and the ITWs which are associated with the roots of $F^{'}(u) = 0$). However, studies of their stability have revealed a very sensitive dependence on both their initial width, parity, and the width of the lattice, which did not yield itself to a manageable characterization. We leave this topic for future studies. Finally, we also note a class of kink-like excitations, that were not discussed in the paper, for which the roots of $F''(u) = 0$ play a key role.

Acknowledgments

AP is supported in part by the Laboratory of Dynamical Systems and Applications NRU HSE of the Ministry of Science and Higher Education of the Russian Federation (Grant No. 075-15-2019-1931). AP thanks A Slunyaev and E N Pelinovsky for useful discussions.

ORCID iDs

Arkady Pikovsky https://orcid.org/0000-0001-9682-7122

References

[1] Flach S 1995 *Phys. Rev.* E **51** 1503
[2] Dey B, Eleftheriou M, Flach S and Tsironis G P 2001 *Phys. Rev.* E **65** 017601
[3] Rosenau P and Pikovsky A 2005 *Phys. Rev. Lett.* **94** 174102
[4] Rosenau P and Schochet S 2005 *Phys. Rev. Lett.* **94** 045503
[5] Rosenau P and Schochet S 2005 *Chaos* **15** 015111
[6] Pikovsky A and Rosenau P 2006 *Physica* D **218** 56
[7] Herbold E B and Nesterenko V F 2007 *Phys. Rev.* E **75** 021304
[8] Ahnert K and Pikovsky A 2009 *Phys. Rev.* E **79** 026209
[9] Rosenau P and Pikovsky A 2014 *Phys. Rev.* E **89** 022924
[10] Rosenau P and Zilburg A 2016 *Phys. Lett.* A **379** 2811
[11] Zilburg A and Rosenau P 2015 *J. Phys.* A **49** 095101
[12] James G 2018 *Phil. Trans. R. Soc.* A **376** 20170138
[13] Campbell D K, Flach S and Kivshar Y S 2004 *Phys. Today* **57** 43
[14] Flach S and Gorbach A V 2008 *Phys. Rep.* **467** 1
[15] Sen S, Hong J, Bang J, Avalos E and Doney R 2008 *Phys. Rep.* **462** 21
[16] James G and Pelinovsky D 2014 *Proc. R. Soc.* A **470** 20130462
[17] Herrmann M 2017 *J. Nonlinear Sci.* **27** 213
[18] Anco S C and Przedborski M 2018 *Phys. Rev.* E **98** 042208
[19] Rosenau P and Pikovsky A 2020 *Chaos* **30** 053119
[20] Slunyaev A 2001 *J. Exp. Theor. Phys.* **92** 529
[21] Grimshaw R, Pelinovsky D, Pelinovsky E and Slunyaev A 2010 *Chaos* **12** 1070
[22] Kamchatnov A M, Kuo Y-H, Lin T-C, Horng T-L, Gou S-C, Clift R, El G A and Grimshaw R H J 2012 *Phys. Rev.* E **86** 036605
[23] Ahnert K and Pikovsky A 2008 *Chaos* **18** 037118
[24] Matheny M H *et al* 2019 *Science* **363** eaav7932
[25] Herrmann M 2014 *Math. Models Methods Appl. Sci.* **22** 1150002
[26] Manakov S V 1975 *Sov. Phys. JETP* **40** 269
[27] Kac M and van Moerbeke P 1975 *Adv. Math.* **16** 160
[28] Rosenau P and Zilburg A 2018 *J. Phys. A: Math. Theor.* **51** 343001
[29] Rosenau P 2003 *Phys. Lett.* A **311** 39
[30] Doedel E J 2007 *Numerical Continuation Methods for Dynamical Systems* ed B Krauskopf, H M Osinga and J Galan-Vioque (Berlin: Springer)
[31] Cai D, Bishop A R and Grønbech-Jensen N 1994 *Phys. Rev. Lett.* **72** 591